Journal of Marine Research, 47, 547–567, 1989

Resonance of internal waves in fjords: A finite-difference model

by Benoit Cushman-Roisin,[1] Vigdis Tverberg[2] and Edgar G. Pavia[1]

ABSTRACT

After the time periodicity is removed from the problem, the spatial distribution of internal waves in a stratified fluid is governed by a hyperbolic equation. With boundary conditions specified all along the perimeter of the domain, information is transmitted in both directions (forward and backward) along every characteristic, and, unlike the typical temporal hyperbolic equation, the internal-wave equation is not amenable to a simple forward integration. The problem is tackled here with a finite-difference, relaxation technique by constructing a time-dependent, dissipative problem, the final steady state of which yields the solution of the original problem.

Attempts at solving the problem for arbitrary topography then reveal multiple resonances, each resonance being caused by a ray path closing onto itself after multiple reflections. The finite-difference formulation is found to be a convenient vehicle to discuss resonances and to conclude that their existence renders the problem not only singular but also extremely sensitive to the details of the topography. The problem is easily overcome by the introduction of friction.

The finite-difference representation of the problem is instrumental in serving as a guide for the investigation of the resonance problem. Indeed, it keeps the essence of the continuous problem and yet simplifies the analysis enormously. Although straightforward, robust and successful at providing a numerical solution to a first few examples, the relaxation component of the integration technique suffers from lack of efficiency. This is due to the particular nature of the hyperbolic problem, but it remains that numerical analysts could improve or replace the present scheme with a faster algorithm.

1. Introduction

A typical hyperbolic problem, with time as one of the independent variables, is constrained by a sufficient number of initial conditions (as many as the order of the problem) but is not subjected to any condition about subsequent states except along the boundaries. This property permits an analytical integration by the method of characteristics or a natural, forward-in-time numerical integration. But, there exist hyperbolic problems where none of the independent variables is time, and for which boundary conditions are imposed all around the domain. An important case is that of

1. Department of Oceanography, Florida State University, Tallahassee, Florida, 32306, U.S.A.
2. Geophysical Institute, Avd. A, University of Bergen and Bergen Scientific Centre, 70 Allegaten, 5007 Bergen, Norway.

internal gravity waves in a stratified fluid, where the wave amplitude, ψ, obeys a second-order hyperbolic equation in the space variables (Baines, 1971, 1982; Craig, 1987):

$$\frac{\partial^2\psi}{\partial x^2} - c^2\frac{\partial^2\psi}{\partial z^2} = 0. \tag{1}$$

In this equation, ψ has time-dependence exp $(-i\omega t)$, x is a horizontal coordinate, z the vertical coordinate, and $c = \omega/N$ where ω is the wave frequency (typically a tidal period) and N is the Brunt-Väisälä frequency. In general, N can be a function of depth, but wave refraction is not the topic of the present paper, and, therefore, N will be taken here as a constant. The reader will find in Appendix A a derivation of Eq. (1) as well as a critical review of its most common generalization.

Eq. (1) is obviously hyperbolic, with characteristic slopes equal to $\pm c$ everywhere. As these sloping characteristics intersect the surface, the bottom topography, and the lateral boundaries, the wave-amplitude pattern consists of a multitude of reflections with constructive and destructive interferences. This is precisely the situation in Norwegian fjords (Cushman-Roisin and Svendsen, 1983, and references therein) where a typical ray slope of internal tides is comparable to the depth-to-length aspect ratio of the fjord and hence also to its bottom slope.

The no-flow condition through the surface and (arbitrary) bottom topography and the in/out-flow condition of the lateral boundaries provide one and only one boundary condition at any point on the perimeter of the domain. No direct integration along characteristics can be started from any side, for such procedure would require at least two boundary conditions along the starting edge.

The above internal-gravity-wave problem is an old and important one (Baines, 1982), but is far from being solved. In particular, it is still not known under which conditions the problem is ill posed (see Section 4 for an elementary example), and existing numerical procedures to this day are much too restrictive. For example, the method of Sandstrom (1976) not only requires considerable preliminary work in constructing a transfer function from the topography function before numerical inversion of a matrix can proceed but also restricts application to subcritical slopes (i.e., bottom slopes everywhere less than the characteristic slope). Although it can handle supercritical slopes, the recent method of Craig (1987) is limited to monotonic topography (the depth can only decrease from one end to the other), and furthermore it, too, requires substantial preliminary work in constructing a set of algebraic equations from characteristics criss-crossing the domain. In both methods, the preliminary task is a cumbersome one and must be redone when the wave frequency (ω) or the stratification parameter (N) are modified. Moreover, both methods suffer another major drawback.

Thin, energetic beams and shocks are expected in solutions of hyperbolic problems. In the case of internal gravity waves, high-energy beams typically originate from

critical and almost critical bottom slopes. Fine resolution is required. However, the work necessitated by the methods of Sandstrom and Craig becomes prohibitively arduous when ten to twenty degrees of freedom are selected in the vertical and, also, the matrices to be inverted become ill posed as adjacent rows become increasingly alike with increasing resolution.

Finally, as this work reveals, multiple resonance is the rule rather than the exception. Friction is necessary to remove the singularities, and thus a pure characteristic method becomes impractical.

Chuang and Wang (1981) must be credited with the first finite-difference numerical method for the solution of internal-wave generation by irregular bottom topography. Their technique relies on a change of coordinates that transforms the domain into a rectangle, which is subsequently divided arbitrarily by evenly spaced grid points. Two arguments can be raised as limitations to this procedure. First, the transformation of coordinate involves the second derivative of the bottom profile and hence limits the applications to smooth profiles or to those with analytical expressions. Second, the aspect ratio of the computational cells is unrelated to the ray slope, and the resulting inter- and extrapolations lead to a certain amount of smoothing and/or noise. For these reasons or perhaps also because their emphasis was on the effect of lateral and vertical inhomogeneities in the stratification, Chuang and Wang (1981) limited their applications to gentle, monotonic and subcritical bottom slopes, thereby eliminating the existence of concentrated beams and of eventual resonances.

All these arguments demonstrate that the classic problem of internal-wave generation by irregular topography has not yet received satisfactory solution and, therefore, calls for the development of a generic numerical method of integration. What is missing is a numerical method of integration with ease of implementation, wide applicability, and a potential for future improvements. Toward fulfillment of this goal, a double transformation of the problem is hereby proposed: first, the original problem is recast as a dissipative problem; then, a classic finite-difference discretization is applied to the continuous system. At the conclusion of the work, it will appear that the finite-difference approach considerably simplifies the problem by providing a helpful framework for the discussion of resonance, but that the relaxation technique for solving the analogous, dissipative problem could be improved.

2. Transformation of the problem

Numerical relaxation techniques, such as successive over-relaxation, have proven to be extremely helpful in solving elliptic equations (O'Brien, 1986). The chief reason for this success lies in the fact that the solution of an elliptic equation can be interpreted as the final, steady-state solution of a time-dependent, dissipative problem; the latter being usually straightforward to integrate. A similar transformation of the hyperbolic problem at hand into a parabolic problem would thus be promising, and is carried out here.

Instead of using the streamfunction ψ as in (1), it has been found more convenient in the analysis that follows to return to the original velocity components $u = -\partial\psi/\partial z$ and $w = \partial\psi/\partial x$. Moreover, as the variables can be scaled (w by c, x by $1/c$), the problem can be formulated as (see Appendix A)

$$\frac{\partial u}{\partial x} + \frac{\partial w}{\partial z} = 0, \qquad \frac{\partial u}{\partial z} + \frac{\partial w}{\partial x} = 0. \tag{2a, b}$$

The characteristic slopes are now ± 1. Boundary conditions include one condition on a combination of u and w on all sides of the domain, for example $w = 0$ ($u = 0$) on horizontal (vertical) sections of the bottom topography.

Because our present goal is to recast (2a, b) into a diffusive problem, we apply the Laplacian operator to u and w and find $\nabla^2 u = -2\partial^2 w/\partial x\partial z$, $\nabla^2 w = -2\partial^2 u/\partial x\partial z$, and formulate the new problem

$$\frac{\partial u}{\partial t} = K\left(\nabla^2 u + 2\frac{\partial^2 w}{\partial x \partial z}\right), \qquad \frac{\partial w}{\partial t} = K\left(\nabla^2 w + 2\frac{\partial^2 u}{\partial x \partial z}\right), \tag{3a, b}$$

where K is an arbitrary positive constant and t a time-like variable. Aside from the coupling terms, the above two equations are obviously dissipative. It now remains to prove that Eqs. (3a, b) with the coupling terms still form a dissipative system, and that their steady-state solution, with the appropriate boundary conditions, is the solution to Eqs. (2a, b).

In order to demonstrate the first assertion, we decompose the solution in modes of the form $\exp(\sigma t + imx + inz)$. For arbitrary real values of m and n, Eqs. (3a, b) provide the values of σ

$$\sigma = -K(m \pm n)^2, \tag{4}$$

which are real and nonpositive. Neither growth nor oscillations can exist, and the solution progresses toward a steady state. Note, however, that σ is zero for $m/n = \pm 1$, and no dissipation occurs in the direction of the characteristics.

To demonstrate the equivalence between the steady state of Eqs. (3a, b) and the solution of Eqs. (2a, b), and in anticipation of the numerical implementation, two accessory functions are defined

$$\chi = \frac{\partial u}{\partial x} + \frac{\partial w}{\partial z}, \phi = \frac{\partial u}{\partial z} + \frac{\partial w}{\partial x}, \tag{5a, b}$$

which are used to rewrite Eqs. (3a, b) with first-order derivatives only

$$\frac{\partial u}{\partial t} = K\left(\frac{\partial \chi}{\partial x} + \frac{\partial \phi}{\partial z}\right), \frac{\partial w}{\partial t} = K\left(\frac{\partial \chi}{\partial z} + \frac{\partial \phi}{\partial x}\right). \tag{5c, d}$$

The set of equations (5a) to (5d) forms a 4×4 system for the functions u, w, χ and ϕ. It is of fourth order and requires two boundary conditions all around the perimeter of the

domain. The one boundary condition on u and w of the original problem (2a, b) is retained, and a second condition on χ and ϕ is now added. Since Eqs. (5a, b) indicate that χ and ϕ should be zero to recover Eqs. (2a, b), the second boundary condition is taken as homogeneous, but it needs not be written down explicitly at this time.

With arbitrary (guess) initial values for u, w, χ and ϕ, the diffusive system (5a–d) equilibrates to a steady state, at which time the temporal derivatives have vanished. From Eqs. (5c, d), it remains $\partial\chi/\partial x + \partial\phi/\partial z = 0$ and $\partial\chi/\partial z + \partial\phi/\partial x = 0$ and, because of the homogeneous nature of the boundary conditions of χ and ϕ, the unique solution to this hyperbolic problem is $\chi = \phi = 0$. Eqs. (2a, b) are thus recovered, and the steady-state solution of the dissipative problem is indeed the solution to the original problem.

There is, however, a notable exception to the preceeding argument. Indeed, in the eventuality of the existence of one or more closed ray paths, a nonzero solution to the χ-ϕ problem may exist. This resonance phenomenon will be investigated in the context of the numerical procedure, where the finite-difference technique adds clarity to the problem.

3. Relaxation technique

The derivatives in Eqs. (5a–d) make it ideal to use a staggered grid as displayed in Figure 1. Let Δ be the grid interval. One numerical array $A(i, j)$ suffices, with the $u(w)$ values occupying the even-even (odd-odd) positions and the $2\Delta\chi$ ($2\Delta\phi$) values occupying the odd-even (even-odd) positions. (The factor 2Δ is introduced for convenience.) All derivatives in Eqs. (5a–d) can then be evaluated as centered differences with second-order accuracy. Both diagnostic equations (5a, b) take the same form:

$$A(i, j) = A(i + 1, j) + A(i, j + 1) - A(i - 1, j) - A(i, j - 1), \tag{6}$$

with i or j even and the other odd. The prognostic equations (5c, d) can be marched by a forward time step (with again one form for both equations)

$$\text{new } A(i, j) = A(i, j) + \frac{K\Delta t}{4\Delta^2}[A(i + 1, j) + A(i, j + 1) - A(i - 1, j) - A(i, j - 1)], \tag{7}$$

with i and j both even or odd. The inaccuracy in the forward time stepping is inconsequential, for only the final, steady state matters.

The numerical stability of this relaxation scheme can be evaluted by the traditional method. For $\alpha = m\Delta$ and $\beta = n\Delta$, m and n being the wavenumbers in the x and z directions, the amplification factor at every time step is

$$G = 1 - \frac{K\Delta t}{\Delta^2}(\sin\alpha + \sin\beta)^2. \tag{8}$$

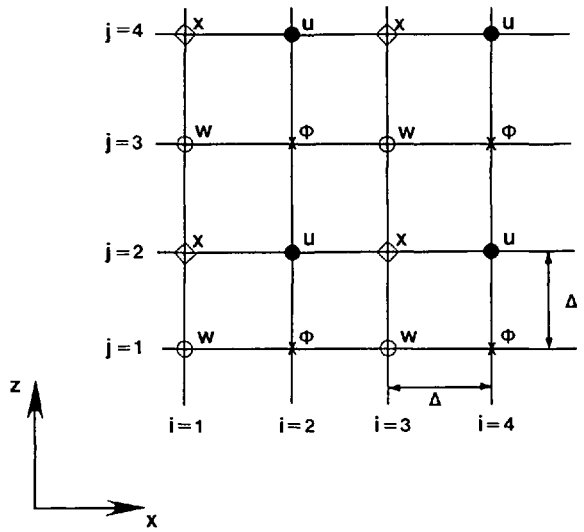

Figure 1. The staggered grid that takes advantage of the form of Eqs. (5a–d). All first-order derivatives can be evaluated by centered differences. Note that because the grid interval is the same in both directions the u and w gridpoints form straight lines of slopes ± 1; i.e., parallel to the characteristics of the problem.

Note the analogy with (4). As $(\sin \alpha + \sin \beta)^2$ varies between 0 and 4, the minimum and maximum values of G are $1 - 4K\Delta t/\Delta^2$ and 1, and the requirement that both be less than or equal to one in amplitude brings the condition on the time step

$$\frac{K\Delta t}{\Delta^2} \leq \frac{1}{2}. \tag{9}$$

It now remains to discuss the placing of the grid in the computational domain and the implementing of the boundary conditions. The rectangular gridding of the domain forces us to represent the bottom topography as a series of steps, each of two grid-spacing units (2Δ). Figure 2 provides an example. Horizontal segments of the topography are chosen to pass through w-gridpoints where w is set to zero and, similarly, vertical segments intercept u-gridpoints where u is set to zero. The intermediate gridpoints along the bottom are naturally ϕ-gridpoints (see Fig. 2), and ϕ is then set to zero at these boundary points. The grid ends at the surface with a horizontal row of w and ϕ points. There, w is set to zero (if the forcing is a set of internal modes incoming from a side) or to a constant, say unity (if the forcing is the external tide, see Craig, 1987); ϕ is set to zero along the surface. The lateral extremities of the system can be either closed (topography rising to the surface) or open, with at least one side open to let the tidal signal come in. The closed extremity, if there is one, is treated as a vertical extent of the bottom topography, while the open extremities are boundaries where the physics dictate a condition on w, either incoming external tide

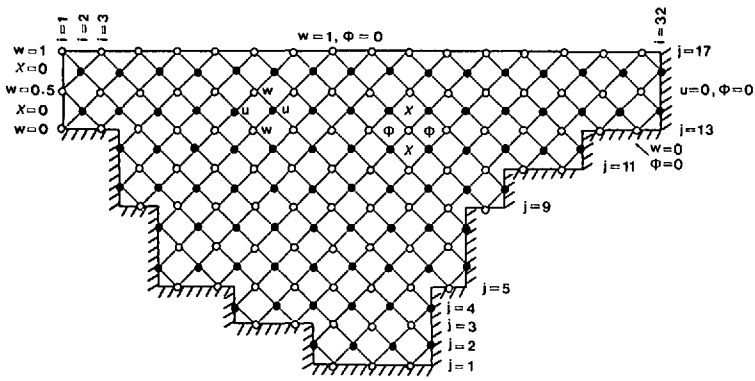

Figure 2. An example of a discretized system. Note that, with the exception of the entrance (left side of figure), all boundary points are chosen such as the w (u) points fall on horizontal (vertical) boundary segments. Naturally, all intermediate boundary gridpoints are ϕ points. Along the entrance, w and χ points take the place of the u and ϕ points. One equation of type (5a, b) can be written for every complete interior diamond, and one equation of type (5c, d) can be written for every interior node.

with reflection of the internal modes (w given decreasing from the surface value linearly to zero at the bottom) or a radiation boundary condition. Since our present objective is to develop a generic technique of integration and to analyze the problem of resonance in the interior of the domain, we choose for the open-boundary condition to set the vertical velocity equal to that of the external tide and to let the internal modes be reflected. The implementation of the more appropriate radiation condition is postponed to a future article. As the χ-gridpoints are located vertically between the gridpoints, every other gridpoint along the entrance is a χ-gridpoint, and χ is set to zero there.

So implemented in the domain, the grid forms a network of diamonds with the u and w unknowns at the corners (Fig. 2). For every complete interior diamond, an equation of type (2) can be written, and a necessary condition for a well-posed problem is that there be equal numbers of such diamonds (equations) and of interior points (unknowns). Appendix B demonstrates, for arbitrary geometry, that this is indeed the case.

Initial conditions are required to start the iterative integration, but these can be arbitrary. One choice is $u = w = \chi = \phi = 0$ everywhere in the interior.

Finally, since ϕ and χ should tend to zero as the steady state is approached, their maximum value is an indication of the progress toward the solution. We therefore define the dimensionless residual

$$R = \frac{\max_{\chi,\phi} |A(i,j)|^2}{\frac{1}{N}\sum_{u,w} |A(i,j)|^2} \tag{10}$$

where the search for the maximum in the numerator covers the (even, odd) and (odd, even) pairs of indices, the sum in the denominator covers the (even, even) and (odd, odd) pairs of indices, and N is the number of unknowns in the problem (u and w values only).

4. Resonance—an example

As was indicated earlier in the text, resonances can be anticipated. For example, if we trace the ray paths (diagonal lines) of Figure 2, continuing the path by a 90°-turn at every reflection, we find that three independent paths are needed to cover all grid points: one starts and ends at the open boundary (on the upper left), while the other two are closed onto themselves. Numerical experiments strictly following the procedure outlined above showed convergence to a steady state solution, but that solution had nonzero values for ϕ and χ. Remarkably enough, the same nonzero χ and ϕ values were recurring—two distinct values and their sum—indicating that perhaps each value had a relation to a closed ray path.

To elucidate the question further, a very simple example is now constructed. Displayed in Figure 3, the small grid contains only six unknowns (four u-values and two w-values), but two ray paths exist. First, to demonstrate that resonance is not a spurious phenomenon brought on by the transformation of the problem into a dissipative system, we ignore for the moment the ϕ and χ notation, and write the discretized versions of (2a, b) for each interior diamond:

$$1 + u_2 = u_1 + 0,\ 1 + u_3 = u_2 + w_1,\ 1 + 0 = u_3 + w_2$$
$$u_3 + w_2 = w_1 + u_4,\ w_1 + u_4 = 0 + 0,\ w_2 + 0 = u_4 + 0.$$

Inspection of this 6×6 linear problem shows that the third, fourth and fifth equations add up to $1 = 0$, i.e., the determinant is zero, and no finite solution exists. Now, introducing the χ and ϕ variables and writing Eqs. (6) and (7), we find that the steady state has the following properties: the three χ values outside of the closed ray path are zero while the two χ values and the ϕ value inside the closed ray are equal to $\frac{1}{3}$. The values of u_1 and u_2 are determined (7/3 and 4/3, respectively), while the values of u_3, u_4, w_1 and w_2, i.e., the unknowns along the closed ray path, are left undetermined (one of the four can be chosen arbitrarily). What these values would be as the result of a computer iteration is dependent on the initial guess values.

With nonzero values of χ and ϕ, the preceeding solution does not satisfy the equations (2a, b) of the original problem, and cannot be accepted. However, we are now convinced that the singularity of the problem is intimately related to the existence of the closed ray path, and we intuitively anticipate that problems with greater dimensions will likely exhibit similar singularities; namely, due to resonant (closed) ray paths.

The greater the dimensions of the problem (i.e., the finer the numerical resolution), the greater the chance that closed paths exist. Therefore, resonance is most likely the rule rather than the exception, and the problem is aggravated in the theoretical limit to

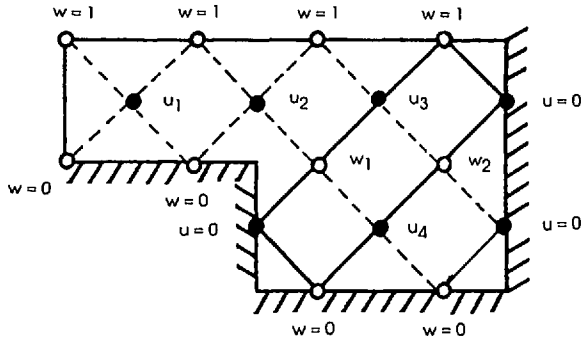

Figure 3. A simple example illustrating resonance. Note the two independent ray paths: one (dashed line) starts and ends at the open boundary (left side), while the other (solid line) closes on itself.

the continuum. This, in turn, suggests that the nature of resonance is not caused by the present finite-difference scheme but is rather an intrinsic characteristic of the physical problem at hand. Quite the contrary, the finite-difference scheme is a simplifying factor.

Finally, adding or subtracting small topographic features may thoroughly change the number and/or configuration of the resonant ray paths, indicating that the internal-wave distribution is greatly sensitive to small topographic features. As an example, the subtraction of the diamond centered at $(i = 7, j = 6)$ in Figure 2 by the addition of a bottom kink raises the number of independent rays from three to four.

For all the above reasons, it is imperative that the resonance problem be overcome, and it is clear that a physical, not a numerical, remedy should be applied. A logical antidote, which will couple the information across the closed ray paths, and which will at the same time lessen the critical sensitivity of the solution on the details of the topography, is the introduction of dissipation.

It is worth noting here that a necessary condition for the existence of a resonant ray path is the existence of at least two facing supercritical slopes (so that a forward ray can be reflected first backward and then forward again), and that all previous models carefully avoided such a situation. Wunsch (1968), Baines (1974, 1982) and Craig (1987) all restricted their analyses to monotonic slopes, while Baines (1971) investigated the problem of a topographic bump; i.e., that of two oppositely facing slopes, and Sandstrom (1976) considered only subcritical slopes.

In closing, it should be pointed out that, although existence of closed rays and ill-posedness go hand in hand for the discretized problem, a general rule to determine under which conditions the continuous problem is ill posed has yet to be formulated.

5. Overcoming resonance

The previous section demonstrated the likelihood of resonance in any problem of sizeable dimension and illustrated the resulting mathematical singularity. It was

suggested that the physical nature of the problem calls for the addition of a physical process, namely dissipation. This process is to be distinguished from the dissipative-like behavior introduced in Section 2. There, no additional physical mechanism was injected in the equations, and dissipation strictly referred to spreading of information during the unfolding of the numerical, time-like variable. The task of including vertical viscosity is now undertaken.

With a temporal dependence of the type exp $(-i\omega t)$ where ω is the tidal frequency and with the inclusion of vertical viscosity, the primitive equations are:

$$-i\omega u = -p_x + \nu u_{zz} \tag{11a}$$

$$0 = -p_z + b \tag{11b}$$

$$-i\omega b + N^2 w = 0 \tag{11c}$$

$$u_x + w_z = 0, \tag{11d}$$

where all symbols are as previously defined (see Appendix A), with the addition of ν, the vertical viscosity. Although one could conceive of including diffusion of buoyancy as an additional dissipative mechanism, it is not necessary, since the diffusive time scale for density is much greater than that for momentum. It is also inadvisable since the entire linear theory of internal waves is based on the existence of a background vertical stratification that is neither eroding in time nor supported by a constant vertical buoyancy flux.

Estimates of the eddy viscosity (Knauss, 1978) range from 10^{-4} to 10^{-3} m^2 s^{-1}. With a frequency corresponding to the semi-diurnal tide ($\omega \sim 2\ 10^{-5}$ s^{-1}) and the fjord depth of one to several hundred meters, ωH^2 is on the order of 1 m^2 s^{-1}, and one thus notes the strong inequality

$$\nu \ll \omega H^2, \tag{12}$$

which implies that the effect of friction will be negligible except in those areas where it plays a crucial role in removing resonance.

Eq. (11c) yields $b = -iN^2 w/\omega$, while the cross-differentiation of (11a) and (11b) eliminates the pressure. The resulting equation is:

$$c^2 u_z + w_x = i\lambda u_{zzz}, \tag{13}$$

where $c = \omega/N$ and where $\lambda = \nu\omega/N^2$ is a small, real, positive constant coefficient. Inequality (12) implies that λ be much smaller than $c^2 H^2$.

Eq. (13) combined with the continuity equation (11d) forms again a two-by-two system for u and w. Scaling the variables w by c, x by $1/c$, as performed in Section 2, and λ by c^2, we obtain the following system of equations, which now supersedes

(2a, b):

$$\frac{\partial u}{\partial x} = \frac{\partial w}{\partial z} = 0, \qquad \frac{\partial u}{\partial z} + \frac{\partial w}{\partial x} = i\lambda \frac{\partial^3 u}{\partial z^3}, \tag{14a, b}$$

with the proviso $\lambda \ll H^2$.

In analogy with the relaxation method introduced in Section 2, the problem is then transformed into the following system of equations

$$\chi = \frac{\partial u}{\partial x} + \frac{\partial w}{\partial z} \tag{15a}$$

$$\phi = \frac{\partial u}{\partial z} + \frac{\partial w}{\partial x} - i\lambda \frac{\partial^3 u}{\partial z^3} \tag{15b}$$

$$\frac{\partial u}{\partial t} = K\left(\frac{\partial \chi}{\partial x} + \frac{\partial \phi}{\partial z}\right) \tag{15c}$$

$$\frac{\partial w}{\partial t} = K\left(\frac{\partial \chi}{\partial z} + \frac{\partial \phi}{\partial x} + i\lambda \frac{\partial^3 \chi}{\partial z^3}\right), \tag{15d}$$

where t is a numerical time of integration. For a solution of the type $\exp(\sigma t + imx + inz)$, the constant σ is found to be

$$\sigma = -K\left[m^2 + n^2 \mp 2mn\left(1 - \frac{n^6\lambda^2}{4m^2}\right)^{1/2}\right], \tag{16}$$

and it is not difficult to show that its real part is always negative for nonzero λ. The system (15a–d) is dissipative, and its solution must evolve toward a steady state. Maximum damping without oscillations occurs for those wavenumbers with $n^6\lambda^2/4m^2 = 1$, and, for the smallest scale ($m = n = 2\pi/2\Delta$), we obtain $\lambda \simeq \Delta^2/5$. Numerical experiments with the grid displayed on Figure 2 showed that this value was too small to remove resonance from the problem, while the value $\lambda = \Delta^2/3$ and larger values did lead to convergence toward an acceptable final state ($\chi = \phi = 0$). Note that any value of λ on the order of Δ^2 meets the criterion $\lambda \ll H^2$, for Δ is much less than H in a typical grid.

An analysis of the vertical scales of the system (15a–d) reveals the existence of boundary layers of thickness $\lambda^{1/2}$. These may occur at the bottom, the surface and perhaps also in the interior at the edge of high-energy beams (otherwise discontinuities in the inviscid problem). With λ chosen as small as possible, i.e., on the order of Δ^2, these boundary layers have a thickness comparable to the grid size and are thus poorly resolved. However, a detailed analysis (not reported here) shows that, not unlike classic Ekman layers, the role of these boundary layers is to generate, for the interior, an additional vertical velocity component. The magnitude of this velocity is proportional to $\lambda^{1/2}$, and the numerical representation of the boundary layer with only one grid mesh

solely affects the coefficient or proportionality. Since ν is not precisely known, λ is undetermined within an order of magnitude, and the accurate numerical resolution of the boundary layer is not necessary.

The new system of equations is of eighth order in the vertical, and four boundary conditions are required on the bottom and at the surface. In addition to $w = 1$ and $\phi = 0$ along the surface, we can impose a no-stress condition $u_z = 0$ and, to preserve some symmetry in the problem, $\chi_z = 0$. On the horizontal sections of the bottom, in addition to $w = 0$ and $\phi = 0$, we can impose a no-slip condition $u = 0$, and, by analogy, $\chi = 0$. The boundary conditions on ϕ and χ are clearly irrelevant, for ϕ and χ will vanish everywhere when the steady-state solution is reached. At most, they can affect the rate of relaxation.

The additional boundary conditions are easily implemented by creating two additional, fictitious rows of u and χ gridpoints, one above the surface and one below every horizontal stretch of the bottom. The u and χ values on the former row are set equal to those values on the row just below the surface, while the u and χ values on the latter row segments are set equal and opposite to those values immediately above the bottom.

6. Numerical experiments

Three computational experiments were performed in order to test the finite-difference technique. The first one is a relatively simple problem without resonance and for which an analytical solution is available. Figure 4 displays the analytical solution, its streamfunction contours and the numerical solution obtained with a purposefully coarse resolution of the topography. The excellent agreement supports the present method of solution. Notwithstanding the authors' efforts, no other nontrivial analytical solution has been found, and therefore further testing was not possible.

The second experiment corresponds to the example displayed in Figure 2. The forcing is the external tide ($w = 1$ along the surface gridpoints), the bottom slope varies in sign and amplitude, and the number of interior points (i.e., number of unknowns) is 131. For this example, the methods of Sandstrom (1976) and Craig (1987) are not applicable, for on one hand, some segments of the bottom topography, those with slopes 2 to 1, are supercritical, and, on the other hand, the bottom topography is not monotonic.

On the contrary, the present method is applicable to the chosen, irregular topography, and the coding of the latter to determine the range of the do-loops in the algorithm is straightforward. The numerical computations start with an initial value of R, as defined by (10), of 435.53. As the iterations are performed, the residual R drops monotonically and, after a certain number of iterations, decays according to an exponential function, presumably that of the slowest decaying mode. Calculations reveal that the χ values during the relaxation process are not distributed evenly about a zero mean, and, as a result, the errors on mass continuity add up from cell to cell to a

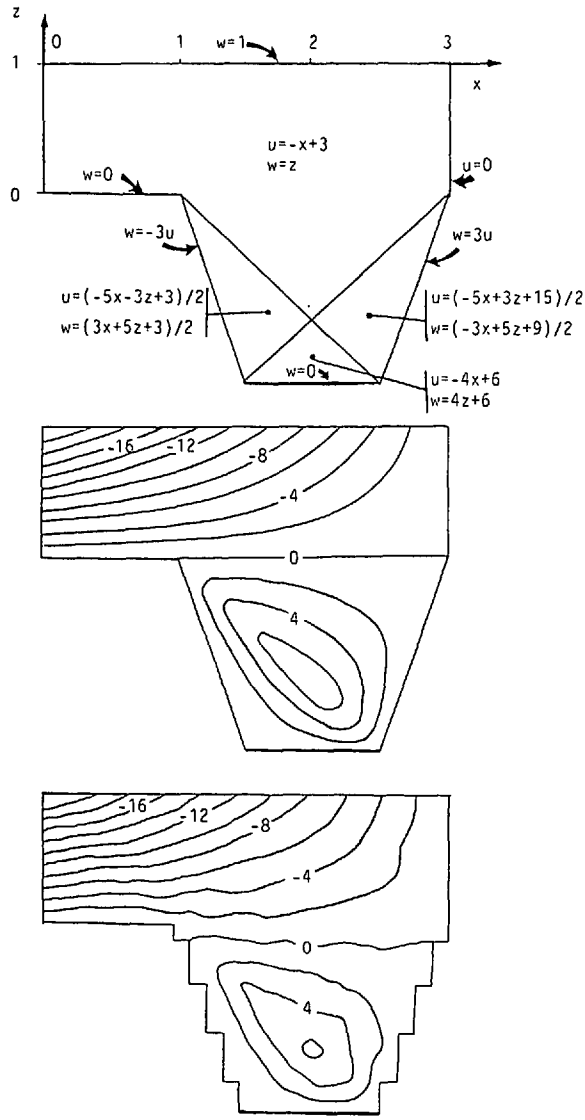

Figure 4. Comparison between analytical and numerical solutions. Top panel: the analytical solution; middle panel: streamfunction contours from analytical solution; bottom panel: streamfunction contours from numerical solution.

sizeable mass imbalance in the intermediate flow fields. To ensure that in the final flow field the cumulated mass imbalance (calculated as the sum of the errors on Eq. (14a) over all cells) be less than one percent, 27,139 iterations are required by which time the residual R has dropped to $3.75\ 10^{-6}$. The streamfunction field of the solution, $Re[\psi \exp(-i\omega t)]$, is presented on Figure 5.

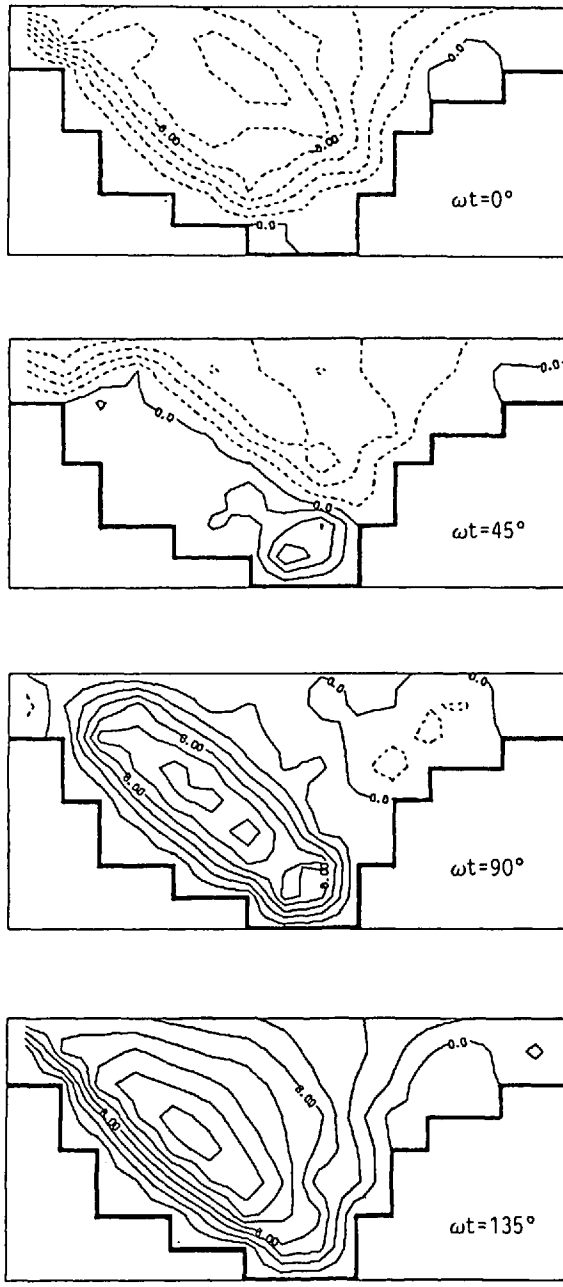

Figure 5. Streamfunction for the solution of the problem presented in Figure 2 (first half of the tidal cycle).

The remark that the χ values tend to be distributed about a nonzero mean is reminiscent of the elementary problem exposed in Section 4, and a heuristic argument can be developed to show that this is a general property. The *inviscid* problem leads to a steady-state solution which, if it contains a closed ray, has nonzero values of χ and ϕ along that ray. The closed ray is made of branches sloping in both the $+1$ and -1 directions, with $\chi + \phi$ constant along one set of branches and $\chi - \phi$ constant along the other. Let us now assume that one branch has $\chi + \phi = a$, where a is a constant. Since the boundary conditions on ϕ are $\phi = 0$, it follows that all other branches of the closed ray are characterized either by $\chi - \phi = a$ or $\chi + \phi = a$, depending on their slope. Now, these branches of the closed ray are traversed by characteristics not belonging to closed rays and thus for which $\chi + \phi = 0$ and $\chi - \phi = 0$ (see example treated in Section 4), and it immediately follows that such intersection points have $\chi = a/2$ and $\phi = \pm a/2$. Where the closed ray intersects itself, $\chi = a$ and $\phi = 0$. If there exists a second closed ray, characterized by the value b, χ can now take the values b, $b/2$ and $(a + b)/2$, while the ϕ values are $\pm b$, $\pm b/2$, $\pm(a + b)/2$. Hence, unlike ϕ, χ assumes a restricted number of values, and it is no wonder that they tend to be scattered around a nonzero mean. With the inclusion of friction, such a situation is not allowed to persist, and all values of χ must ultimately decay below any given threshold. But, by virtue of the smallness of the viscosity coefficient, an adjustment toward the inviscid solution first takes place, and then a slow decay proceeds. This explains why the χ values tend to be clustered around a nonzero-mean during most of the calculations.

A third numerical experiment was designed to test the relaxation technique under finer resolution. The new grid, resembling the depth profile of a Norwegian fjord (Cushman-Roisin and Svendsen, 1983) with a tidal period of 12.42 hours and a Brunt-Väisälä frequency of $9.4\ 10^{-3}\ s^{-1}(c = 0.015)$, has $\Delta z = 5$ m, $\Delta x = \Delta z/c = 333$ m, and 805 unknown values of u and w. In anticipation of a large number of iterations, the relaxation is accelerated by taking λ initially equal to Δ^2 and decreasing it progressively to $\Delta^2/3$. After 180,333 iterations, the flow field has a cumulated mass imbalance of one percent, and the residual R has dropped from an initial value of 834. to $1.52\ 10^{-7}$.

The streamfunction field of the solution, $Re[\psi \exp(-i\omega t)]$, displayed on Figure 6, shows a splitting of the internal-wave field in two branches, both originating at the sill, one pointing upward to be reflected by the surface, and the other pointing downward to be reflected by the bottom. Such feature, including a relatively quiescent zone at sill depth slightly in-fjord of the sill, is precisely what the data (Cushman-Roisin and Svendsen, 1983) revealed. However, a close comparison of the model with the data is premature until the entrance boundary condition allows for outward radiation of internal waves.

7. Conclusions

The problem of internal gravity waves in a stratified fluid leads to a second-order hyperbolic equation accompanied by one and only one boundary condition all around

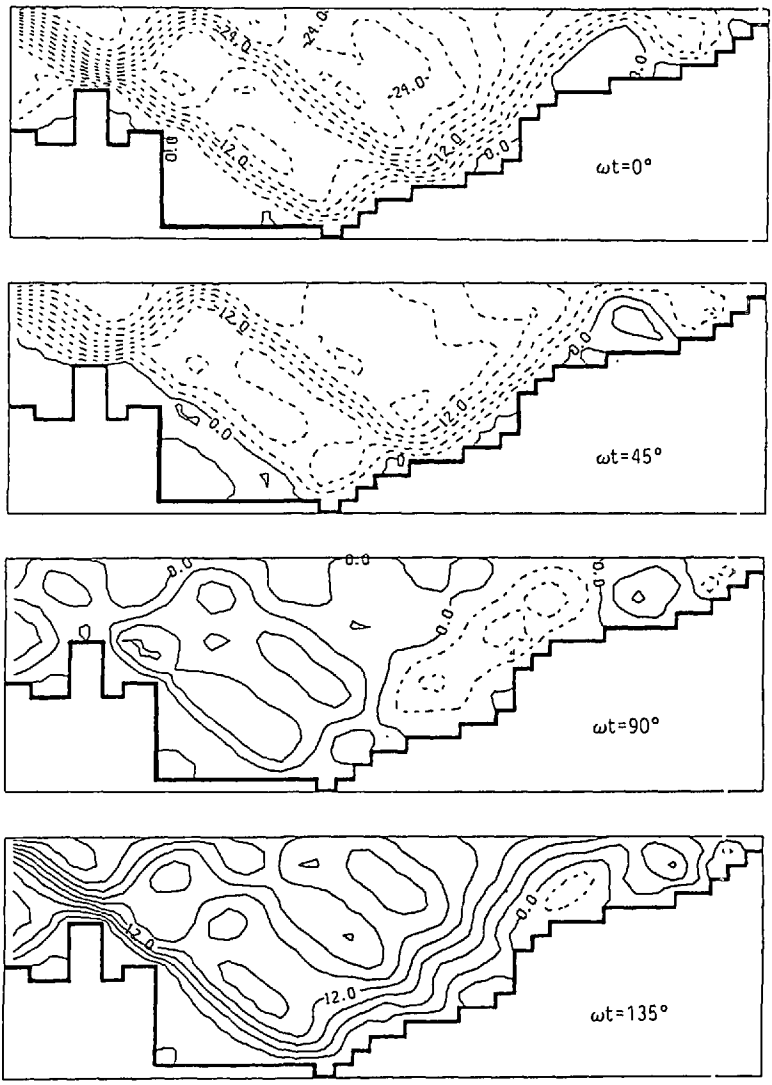

Figure 6. Streamfunction of the second, higher-resolution numerical experiment (first half of the tidal cycle). The topography is not monotonic and contains subcritical as well as supercritical segments.

the perimeter of the domain. This unusual hyperbolic problem cannot be solved by a one-sweep numerical integration following the characteristics. Because the existing methods (Sandstrom, 1976; Craig, 1987), which rely on a one-time matrix inversion, not only present great difficulties in preparing the problem for the computer but also suffer from restricted applicability to special cases from which resonance is excluded, an alternative, simple-minded procedure is devised. The idea lies in discretizing the

domain by means of a staggered grid and in constructing a time-dependent, dissipative problem, the final steady state of which corresponds to the solution of the original problem. This task is accomplished by doubling the order of the problem and adding time derivatives at judicious places in the new equations. Although the order of the problem is raised, the modifications facilitate the formulation of a numerical algorithm, and, not least of all, permit the investigation of the resonance problem in a simplified context.

This numerical procedure exemplifies the problem of resonance, whereby ray paths close onto themselves after multiple reflections. It is argued that resonant ray paths become the rule rather than the exception as resolution increases and the discretized system approaches the continuum. Consequently, a small amount of friction is introduced and this is done at little cost to the numerical procedure. However, it is worth noting that the slightest amount of friction precludes the application of the method of characteristics, on which previous attempts were based.

Two numerical integrations with nonmonotonic bottom slopes and a variety of subcritical and supercritical slopes illustrate the implementation of the relaxation technique. The number of iterations required to reach a global accuracy equal to one percent (see text for definition) is large in comparison with elliptic problems of similar size. The reason lies in the fact that dissipation is weak, and thus convergence is slow along the characteristic directions. In contrast, elliptic problems solved by relaxation techniques lead to fast relaxation rates in all directions. It is hoped that the clarification of the resonance problem by means of the present finite-difference method will serve as a guide in the development by numerical analysts of other, more efficient techniques of solution.

The present method is directly applicable to the study of internal tides in fjords. Contrary to existing methods, no restriction is placed on the nature of the topography, and, like the existing methods, a variation of the tidal frequency and/or the stratification parameter requires a re-coding of the problem. However, in the present case, this task merely amounts to re-discretizing the topography on a grid with a different aspect ratio, and this task could be automated if desired.

The open-boundary condition used in the present article reflects the baroclinic modes and should be amended into a radiation condition that permits leakage of internal-wave energy outward. This was not done here to emphasize the finite-difference approach and the problem caused by resonance. Extension to nonuniform vertical stratification (N and c functions of depth) can be handled by the use of a grid with variable spacing in the vertical, such that, everywhere, diagonals of the grid mesh are parallel to the local characteristics. Both generalizations are now in the works and will be reported in subsequent articles. Finally, extension to include Coriolis effects can also proceed, but, as pointed out in Appendix A, this should include the insertion of a Coriolis term in the vertical balance of forces, and the existing models are not satisfactory in this respect.

Acknowledgments. This research was supported by the Bergen Scientific Centre (Norway) and by a contract from the Office of Naval Research (USA). The authors wish to thank P. Gaffney and H. Svendsen for their hospitality and helpful comments. The expertise of W.H. Heil in formulating the topological problem and its solution (Appendix B) and the perspicacious comments of the editor are deeply appreciated. This article constitutes contribution no. 276 of the Geophysical Fluid Dynamics Institute at the Florida State University.

APPENDIX A

Derivation of the basic equation and discussion of its generalizations

With the temporal dependence of the problem eliminated by the introduction of the tidal frequency ω, the linearized primitive equations are:

$$-i\omega u = -p_x \tag{A1}$$

$$0 = -p_z + b \tag{A2}$$

$$-i\omega b + N^2 w = 0 \tag{A3}$$

$$u_x + w_z = 0, \tag{A4}$$

where u and w are the horizontal and vertical velocity components in the x and z directions, respectively, p is the dynamical pressure, and b is the buoyancy departure from a basic vertical stratification characterized by the buoyancy gradient N^2. In addition to the assumption of small wave amplitudes (to justify linearization), it has also been assumed that there is no variation in the other horizontal direction, no friction, no diffusion, and no Coriolis acceleration.

Eq. (A4) permits the definition of a streamfunction ψ such that $u = -\psi_z$ and $w = +\psi_x$. Then, elimination of p and b immediately yields Eq. (1) of the text, with $c^2 = \omega^2/N^2$.

Two sequential generalizations have been proposed. First, it was recognized that the vertical acceleration must be retained if the oscillation frequency, ω, approaches the Brunt-Väisälä frequency, N. Adding the term $-i\omega w$ on the left-hand side of (A2) yields a new equation, identical to (1) but now with c defined as $c^2 = \omega^2/(N^2 - \omega^2)$. This result shows, as a scaling argument would have also revealed, that the relative importance of the vertical acceleration to the gravitational force is ω^2/N^2. For ω and N on the order of 10^{-4} s^{-1} and 10^{-2} s^{-1}, respectively, this is generally a very small correction. However, in the presence of mixed layers, N may locally drop substantially, and the correction may become crucial. In fact, internal waves are not permitted in regions where $N < \omega$, and internal reflection occurs at the level where $N = \omega$.

The next and classic generalization is that of Baines (1971) whereby the Coriolis force is retained. In doing so, the horizontal velocity component, v, in the direction normal to x and z is introduced. Eq. (A1) is replaced by

$$-i\omega u - fv = -p_x \tag{A5}$$

and the balance of forces in the other horizontal direction is stated:

$$-i\omega v + fu = 0. \tag{A6}$$

The result is still an equation identical to (1), but with c defined by $c^2 = (\omega^2 - f^2)/(N^2 - \omega^2)$. The novelty is that ω is now constrained from below as well as from above ($f < \omega < N$).

There is, however, a serious problem with both generalizations. Indeed, the rotation of the earth (of angular frequency Ω) leads to a rotation vector that, in mid latitudes, has both vertical and horizontal (northward) components. The vertical component yields the Coriolis terms retained above (with $f = 2\Omega \sin\theta$, where θ is the latitude), while the northward component yields another Coriolis acceleration term, to be placed on the left-hand side of (A2) and equal to $-f'(u \cos\alpha + v \sin\alpha)$ with $f' = 2\Omega \cos\theta$ and α equal to the angle between the northward and x directions. This is a vertical acceleration, and its relative importance to the gravitational force is f'/N, or about f/N. Consequently, discarding this term while retaining the vertical acceleration term is valid only if $f/N \ll \omega^2/N^2 < 1$. But, for internal tides, f is slightly less than ω, and both these frequencies are much less than N. Hence, the inequalities are rather $\omega^2/N^2 \ll f/N \ll 1$. Both acceleration terms can be neglected vis-a-vis the gravitational force, or, if one wishes to keep the greater of the two, the Coriolis acceleration takes precedence over the vertical acceleration, and not the opposite as Baines (1971, 1982) and his followers (Sandstrom, 1976; Craig, 1987) have done.

APPENDIX B

Well-posedness of the finite-difference problem

The purpose of this Appendix is to demonstrate that the present numerical problem contains equal numbers of equations and unknowns, for arbitrary topography. As discussed in the text, the numerical grid is formed by staggered u and w points, with horizontal (vertical) segments of the boundary intercept $w(u)$ gridpoints, except for a vertical stretch along the entrance which must fall on w-gridpoints. See Figure 2 for an illustration. In the interior, adjacent u and w gridpoints form square diamonds. Since at the center of each *complete* diamond an equation of type (2a) or (2b) can be written, the number of equations is equal to that of diamonds. On the other hand, the number of unknowns is obviously that of interior u and w gridpoints. Well-posedness of the problem thus requires that the number of diamonds (equations) be equal to the number of interior nodes (unknowns). This proposition is demonstrated in a recursive manner.

We first consider the reduced case for which the lateral extent of the domain is that of the original domain but for which the bottom is raised as close to the surface as possible, leaving only one horizontal row of interior u-gridpoints (see Fig. 7a). By inspection, we note without difficulty that the number of complete diamonds is equal to that of interior nodes.

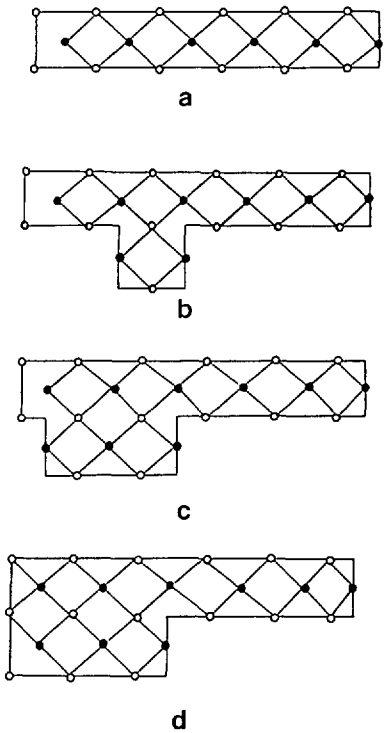

Figure 7. Illustration of the iterative process by which the desired discretization of the topography can be constructed. This demonstrates that the number of equations will always be equal to that of unknowns, regardless of the topography configuration.

We then dig the bottom, unit by unit, until the desired discretization of the topography is obtained. In the digging process, only three moves can occur. The first possible move is to dig a new, one-unit hole in the bottom, as illustrated by passing from Figure 7a to Figure 7b. In the process, one new diamond and one new interior (w) node are created. The second possible move is to enlarge laterally, by one unit, an existing hole, as illustrated by passing from Figure 7b to Figure 7c. In the process two new diamonds and two new interior (u and w) gridpoints are created. The third possible move is to extend laterally an existing hole by half a unit to deepen the entrance, as illustrated by passing from Figure 7c to Figure 7d. In the process, one new diamond and one new (u) node are created.

We then note that, with any move, equal numbers of diamonds and interior points are added. Since the numbers of diamonds and interior points were equal in the initial stage, so they stay throughout the process until the desired discretization of the topography is realized. This proves the stated proposition.

REFERENCES

Baines, P. G. 1971. The reflexion of internal/inertial waves from bumpy surfaces. J. Fluid Mech., *46*, 273–291.

—— 1974. The generation of internal tides over steep continental slopes. Phil. Trans. R. Soc. London, *277A*, 27–58.

—— 1982. On internal tide generation models. Deep-Sea Res., *29*, 307–338.

Chuang, W.-S. and D.-P. Wang. 1981. Effects of density front on the generation and propagation of internal tides. J. Phys. Oceanogr., *11*, 1357–1374.

Craig, P. D. 1987. Solutions for internal tidal generation over coastal topography. J. Mar. Res., *45*, 83–105.

Cushman-Roisin, B. and H. Svendsen. 1983. Internal gravity waves in sill fjords, vertical modes, ray theory and comparison with observations, *in* Coastal Oceanography, H. Grade *et al.*, eds., Plenum Publishing Corp., 373–396.

Knauss, J. A. 1978. Introduction to Physical Oceanography, Prentice-Hall, 338 pp.

O'Brien, J. J., ed. 1986. Advanced Physical Oceanographic Numerical Modelling, D. Reidel Publishing Co., Dordrecht, Holland, 608 pp.

Sandstrom, H. 1976. On topographic generation and coupling of internal waves. Geophys. Fluid Dyn., *7*, 231–270.

Wunsch, C. 1968. On the propagation of internal waves up a slope. Deep-Sea Res., *15*, 251–258.

Received: *6 May, 1988;* revised: *18 May, 1989.*